JOURNAL OF SPACECRAFT AND ROCKETS
Vol. 52, No. 2, March–April 2015

Investigation of Drag-Modulated Supersonic Inflatable Aerodynamic Decelerators for Sounding Rocket Payloads

Matthew J. Miller,* Bradley A. Steinfeldt,† and Robert D. Braun‡
Georgia Institute of Technology, Atlanta, Georgia 30332

DOI: 10.2514/1.A33087

The goal of this investigation is to understand the sizing and performance of supersonic inflatable aerodynamic decelerators for Earth-based sounding rocket applications. The recovery system under examination is composed of a supersonic inflatable aerodynamic decelerator and a guided parafoil system to achieve sub-100 m miss distances. Three supersonic inflatable aerodynamic decelerator configurations (tension cone, attached isotensoid, and trailing isotensoid) are examined using the metrics of decelerator mass, aerodynamic performance, and vehicle integration. In terms of aerodynamic performance, the tension cone is the preferred choice for the sizes investigated. The attached isotensoid was shown to be the most mass efficient decelerator, whereas the trailing isotensoid was found to be the more ideal decelerator for vehicle integration. A three-degree-of-freedom trajectory simulation is used in conjunction with Monte Carlo uncertainty analysis to assess the landed accuracy capability of the proposed architectures. In 95% of the cases examined, the drag-modulated inflatable aerodynamic decelerator provides arrivals within the 10 km parafoil capability region, meeting the sub-100 m landed recovery goals. In 76% of the cases examined, the drag-modulated inflatable aerodynamic decelerator arrives within 5 km of this target zone.

Nomenclature

A	=	area, m^2
C	=	force coefficient
d	=	fabric density, kg/m^2
DR	=	downrange
M	=	Mach number
m	=	mass, kg
q	=	dynamic pressure, N/m^2
S	=	area, m^2
s	=	downrange, m
T	=	reference temperature, K
t	=	time, s
u	=	eastward wind velocity, m/s
V	=	velocity, m/s
v	=	northward wind velocity, m/s
β	=	ballistic coefficient equal to $m/C_D A$, kg/m^2
δDR	=	change in downrange, km
λ	=	launch elevation angle, deg

Subscripts

D	=	drag
deploy	=	deployment
est	=	estimate
f	=	areal
max	=	maximum
min	=	minimum
para	=	parafoil
ref	=	reference
target	=	target

Received 22 June 2014; revision received 22 September 2014; accepted for publication 22 September 2014; published online 2 January 2015.

*Graduate Research Assistant, Daniel Guggenheim School of Aerospace Engineering. Student Member AIAA.

†Research Engineer II, Daniel Guggenheim School of Aerospace Engineering. Member AIAA.

‡David and Andrew Lewis Professor of Space Technology, Daniel Guggenheim School of Aerospace Engineering. Fellow AIAA.

I. Introduction

FIRST proposed in the 1960s, inflatable aerodynamic decelerators (IADs) are devices capable of increasing a vehicle's drag area without the penalty of adding excessive system mass. Compared with conventional parachute technology, IADs are capable of being deployed at higher dynamic pressures and Mach numbers enabling additional deceleration [1]. This study assesses supersonic IADs (SIADs) for Earth-based sounding rocket applications. The analyses presented focus on the SIAD's performance, including landing dispersion, deploy conditions, and system integration considerations.

Numerous flight tests were conducted of these devices until the mid-1970s, examining the aerodynamic drag and stability [2,3]. Typically, SIADs increase the landed mass or landed elevation capability of an entry vehicle on a planetary body. For example, NASA is currently investigating this technology further through the low-density supersonic decelerator program to land larger payload masses on the surface of Mars [4]. Another use of a SIAD is to provide discrete (or continuous) drag modulation as a means of landing site control [5–8]. In this case, SIAD deployment reduces the ballistic coefficient β, providing a means to directly control downrange.

The nominal sounding rocket payload trajectory for this study traverses the Earth's mesosphere at an apogee of 85 km. The particles suspended in the Earth's mesosphere are of scientific interest. Atmospheric particles at these altitudes (45–85 km) have been linked to polar summer mesospheric phenomena such as noctilucent clouds and polar mesosphere summer echoes [9,10]. In addition to Earth-originated material, scientific estimates predict between 10 and 100 t of meteoric material, micron to nanometer in size, enters the Earth's atmosphere per day [11]. Between 2–5% of the matter contained within the mesosphere is estimated to have originated from interstellar space and is highly sought after to further refine the theories and models of the atmospheric and interstellar processes [12,13]. A method for accurately returning high-valued science payloads, such as mesospheric dust, with sub-100 m precision does not exist with current sounding rocket recovery systems. Conventional sounding rocket payload recovery efforts are time and resource intensive. To maximize the science return from captured mesospheric particles, a sub-100 m precision landing requirement is ideal for expedient sample containment, temperature control, and transport to a laboratory facility for processing.

Incorporation of a drag-modulated SIAD as part of a sounding rocket recovery system is not currently offered as a standard recovery option for sounding rockets. The absence of external control surfaces eliminates the need for complicated structural design and actuators for vehicle control, and the absence of reaction control systems with

propellant tanks and propellant greatly simplifies payload packaging, system integration, and mission complexity. Utilization of a SIAD also enables the targeting of staging conditions for additional deployment devices such as a guided parafoil or other subsonic aerodynamic decelerator.

II. System Concept

A. Decelerator Design Space

Various decelerator system architectures were considered from previous work [14]. Figure 1 shows the architectures that were examined. Each architecture uses the launch of a NASA sounding rocket on a suborbital trajectory with an apogee of approximately 85 km. A science payload that captures mesospheric particles operates while the vehicle is above 45 km in altitude. Option 1 uses an existing disk-gap-band (DGB) parachute for supersonic and subsonic descent. This option will serve as a reference baseline for comparison. Options 2–4 use an attached isotensoid, attached tension cone, and trailing isotensoid, respectively. The implications of using each of these devices are considered in this study, from a mass, vehicle integration, and performance perspective. SIAD performance is examined for its downrange control capability through implementation of a drag-modulation algorithm in which the SIAD is deployed at a variable time in-flight. Options 2–4 also incorporate a precision-guided parafoil for terminal accuracy control and controlled descent of the payload.

B. Sounding Rocket Payload Configuration

The proposed architectures are composed of three major components: an Improved-Orion sounding rocket, a cylindrical sounding rocket payload bus, and a decelerator system. The Improved Orion is a NASA sounding rocket that can accommodate a variety of payload diameters, 4.5–17 in., with a bulbous fairing option, and can attain an altitude of 88 km with an 85 lb payload [15]. The flexibility in payload size and mass makes the Improved-Orion sounding rocket an ideal candidate as a mesospheric payload delivery system. The payload bus used in this study is a stock cylindrical bus that has a 14 in. diameter and 47 in. length [15].

C. Decelerator Configurations

The 8.5 m supersonic DGB parachute was selected as a standard configuration from the sounding rocket user's guide [15]. This DGB decelerator option offers a baseline precision recovery performance to which more elaborate recovery configurations are compared.

The three SIADs considered in this study are shown in Fig. 2 in terms of overall dimensions, as well as isometric views integrated with the sounding rocket bus. Work conducted in a previous study [14] was leveraged to establish a baseline size with similar terminal descent velocities (<10 m/s) for each of the SIADs described next.

The tension cone consists of a flexible shell that resists shape deformation by remaining under tension via an inflated torus [16]. The curvature of the tension shell is analytically derived based on a pressure distribution and assumed to have a constant ratio of circumferential to meridional stress. The shell of the tension cone is attached to the forebody at the front of the vehicle and to an inflated torus. An onboard inflation system is required to inflate the torus and to maintain the internal pressure of the torus. The baseline tension cone for this study has an overall diameter of 0.9 m with a torus diameter of 0.1125 m.

The isotensoid configuration is examined as an attached and trailing configuration. The decelerator itself is largely the same for each configuration, except for how the decelerator is integrated with the bus structure. The isotensoid shape enables constant tension throughout the length of the meridians and a uniform biaxial stress across the gore fabric [17]. Ram-air inlets maintain internal pressure of the device, thus no onboard inflation system is required to maintain the inflated shape. However, a preinflation system is typically needed to subject the ram-air inlets to the freestream for inflation to start. The attached isotensoid shape used in this study was derived from the work conducted by Barton in [17] and has a base diameter of 0.9 m. The addition of the burble fence extended the overall diameter of the isotensoid to 0.99 m.

In addition to a preinflation system, the trailing isotensoid is deployed by an ejection event and trails behind the vehicle's bus. The decelerator inflates in a similar manner as the attached isotensoid, except the device is located at some predefined trailing length behind the bus. The representative trailing isotensoid for this study, as shown in Fig. 2, was taken from [18].

To achieve precision landing capability of less than 100 m miss distance, a precision-guided parafoil is used as a terminal decent stage decelerator for this study [19]. A 3.7 m^2 Mosquito Parafoil with a glide ratio of 3 to 1 has been shown to be capable of achieving 100 m landing accuracy if this system is delivered to within 10 km of the target point at an altitude of 6 km [20].

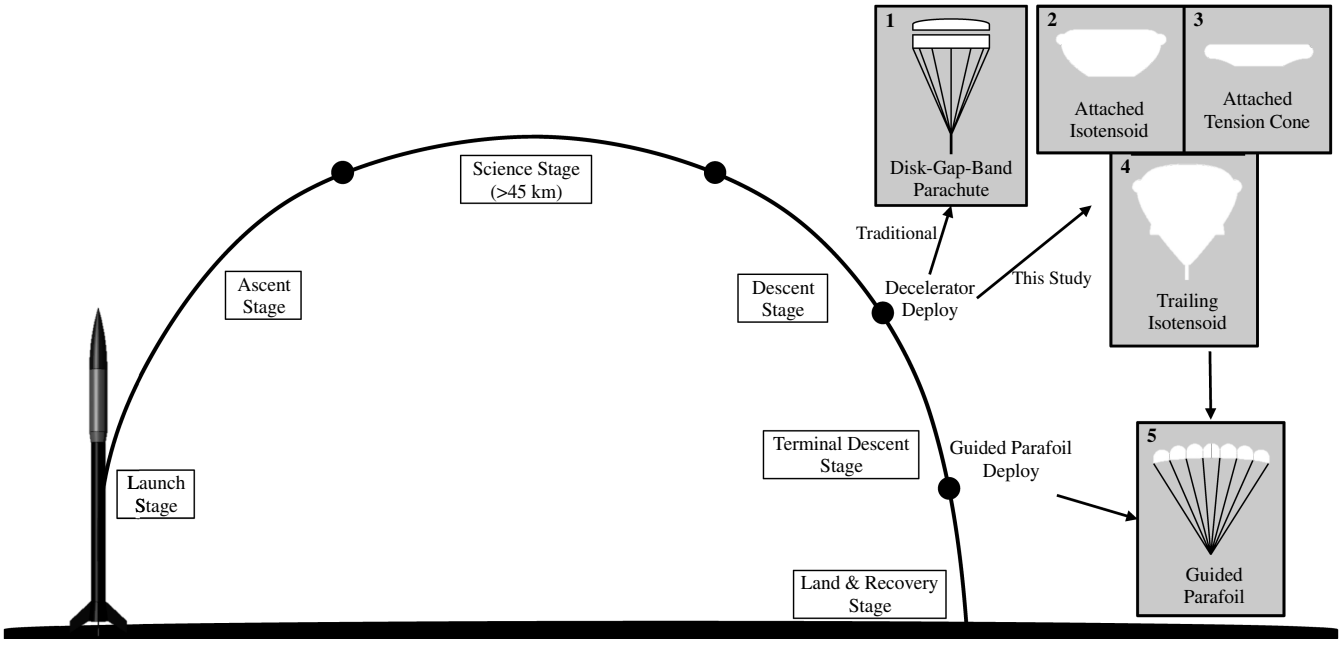

Fig. 1 Mission architecture with focus on supersonic/subsonic decelerator options.

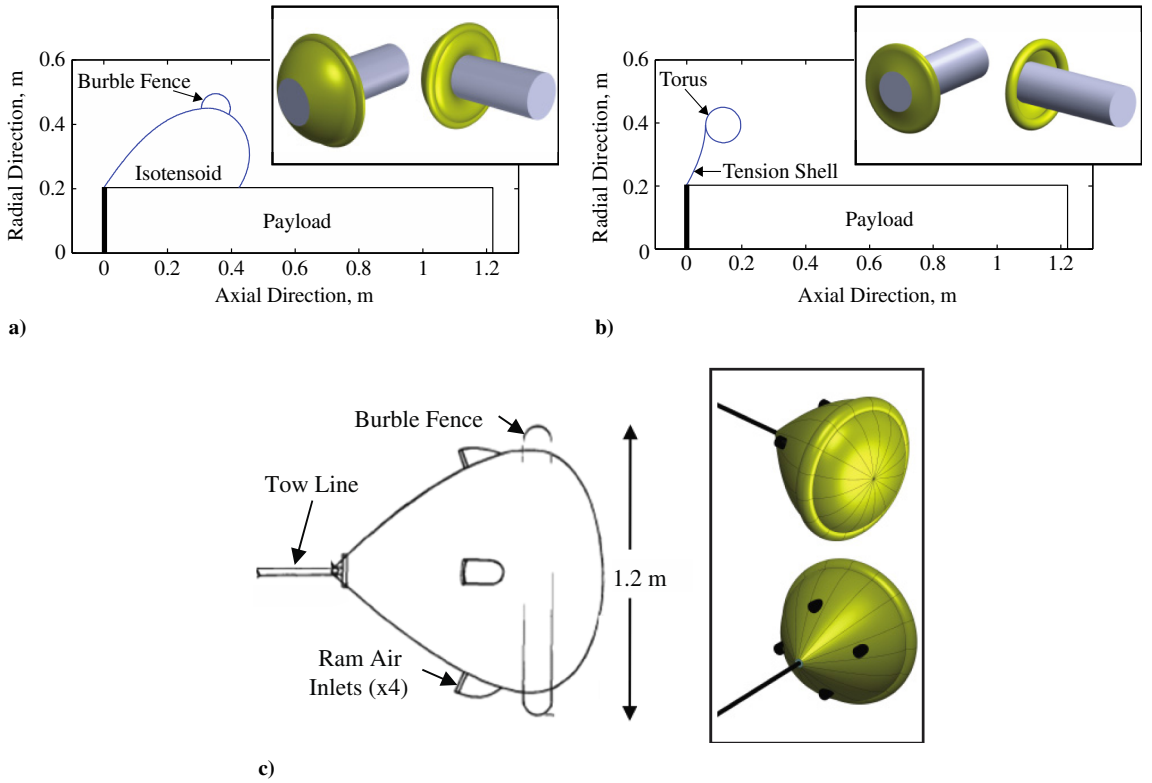

Fig. 2 SIADs a) attached isotensoid, b) attached tension cone, and c) trailing isotensoid.

The three SIADs in this study require different hardware interfaces worthy of some consideration. Table 1 outlines four major mechanisms that are required for proper SIAD function: the attachment, storage, deployment, and inflation mechanisms. These functions provide a starting point to begin considering the integration implications of SIADs on sounding rocket payloads. The attachment mechanism describes the device(s) needed to physically connect to the vehicle bus. The tension cone and attached isotensoid options require fastening the fabric directly to the bus structure, which can be accomplished via the use of a tension hoop. A tension hoop, similar to those found on drums, ensures a secure clamping of the SIAD fabric to the bus structure. The trailing isotensoid can be attached using more conventional devices, such as bridle fasteners.

The storage volume occupied by each SIAD can be calculated using a nominal nonpressurized packaging density of 320 kg/m^3 [21]. The trailing isotensoid can be packaged and stored in the aft of the vehicle bus. The tension cone and attached isotensoid can be stowed on the exterior of the bus structure using a flexible material held together with lacing known as a braided corset [22]. Pyrotechnic cutters can then be implemented to sever the corset lacing to initiate the deployment process of the attached SIADs [23]. The trailing isotensoid can be deployed using a drogue shoot or mortar system [24]. To complete the deployment process, each SIAD must reach full inflation. The tension cone SIAD requires an onboard inflation system. This device comes in various configurations, including a high-pressure vessel gas system or a chemical reaction gas system [22,25]. The isotensoid IADs use an alternative inflation process. They require a preinflation gas system to expose ram-air inlets to the freestream. The preinflation system is usually a small vial of methyl alcohol that provides gas for inflation, once broken [2]. Ram-air inlets, once exposed to the freestream, guide freestream air into the internal structure of the SIAD to complete and maintain internal pressure [26].

III. Modeling and Assumptions

A. Sounding Rocket, Payload Bus, and Decelerator Aerodynamics

This study incorporated Mach-dependent aerodynamics for the sounding rocket and cylindrical bus structure. The drag coefficient values as a function of Mach number for the bulbous sounding rocket payload fairing was estimated to be similar to that of the 5.56 mm BRL-1 ballistic projectile [27], and reference literature was used for the cylindrical bus structure [28]. Because the vehicle is symmetric and assumed to be flying a 0 deg angle of attack, the lift coefficients for the sounding rocket and decelerator are assumed to be zero. The Mach-dependent drag coefficients used in this study for the sounding rocket, bus, and various decelerators are provided in Fig. 3.

For option 1, the stock high-altitude sounding rocket DGB deployed at 73 km altitude with 25 s of inflation time was modeled using a finite-mass inflation curve method [21]. The DGB parachute has extensive flight demonstration and performance capability with upper deployment dynamic pressure and Mach number conditions of 0.9 kPa and 2.5, respectively [29,30]. Limited by the upper mass limit of the 8.5 m DGB, a 24 kg cylindrical bus structure was implemented in this study as the baseline vehicle configuration [15]. SIAD options use deployment dynamic pressure and Mach number limits of 25 kPa and 4.0, respectively. Trailing isotensoid aerodynamic performance was obtained from the already existing literature [31]. The decelerator is placed far enough aft for blunt-body wake effects to be negligible. Guided parafoil deployment constraints of 1.2 kPa dynamic pressure and 0.15 Mach number were also enforced [32].[§]

Computational fluid dynamics (CFD) simulation of the attached SIADs were performed in FUN3D. FUN3D is a fully unstructured three-dimensional fluid solver with both Euler and Reynolds-average Navier–Stokes equation capabilities.[¶] For this preliminary study, Euler solutions were obtained. Grids were generated using Gridgen [33] and consist of between 0.8 and 0.9 million grid points. CFD solutions were generated using the input variable values shown in Table 2, which were chosen as bounding values from the dispersed trajectory.

[§]Data available online at http://www.staratechnologies.com/mosquito.html [retrieved 09 June 2013].

[¶]Data available online at http://fun3d.larc.nasa.gov/ [retrieved 09 June 2013].

Table 1 Decelerator integration mechanisms and descriptions

Mechanism	Tension cone	Attached isotensoid	Trailing isotensoid
		Attachment	
Location	Leading edge	Leading edge	Rear edge
Interface	Single tension hoop	Two tension hoops (one for front surface and one for rear surface)	One or more bridle attachment points
		Storage	
Location	Front (external to bus structure)	Front (external to bus structure)	Rear (internal or external to bus structure)
Devices	Braided corset used to wrap decelerator and fasten to bus	Braided corset used to wrap decelerator and fasten to bus	Packaged similar to that of a small parachute
		Deployment	
Devices	Pyrotechnic cutters used to sever corset lacing and inflation system begins to release pressurized gas	Pyrotechnic cutters used to sever corset lacing and preinflation gas generator releases pressurized gas	Mortar gun ejects small mass to pull decelerator out and preinflation gas generator releases pressurized gas
		Inflation	
Devices	Internal inflation system provides pressurized gas to decelerator	Ram-air inlets guide freestream air into the decelerator	Ram-air inlets guide freestream air into the decelerator

B. Trajectory

A three-degree-of-freedom simulation was used to propagate the trajectory from launch to parafoil deployment. A variable-step, fourth-order Runge–Kutta algorithm with fifth-order error truncation was used, where relative and absolute error tolerances were maintained at 1×10^{-6}. The simulation used an inverse-square law gravity model as well as the Earth–Global Reference Atmospheric Model (GRAM) 2007 [34]. The initial state corresponds to the geographic coordinates of a launch pad at White Sands Missile Range.

C. Drag Modulation Algorithm

Drag modulation is a technique in which the drag area of a vehicle is altered autonomously in-flight as a means of downrange control. In this study, discrete-event drag modulation (SIAD deployment) is used to control vehicle downrange and the subsequent deployment conditions of the parafoil. For a more detailed discussion on drag modulation, refer to [8]. Both a fixed deployment altitude trigger and a predictor–corrector trigger were implemented in this study for range control evaluation. Figure 4 shows the drag modulation guidance logic for the predictor–corrector trigger incorporated into the trajectory simulation.

D. Mass Performance

For each SIAD configuration, the mass was calculated assuming a nominal 0.9-m-diam device. The mass for the tension cone was determined using the dimensionless parameter technique developed in [35]. The total tension cone system's mass was calculated by the summation of eight different dimensionless elements: inflation gas, inflation system mass, toroid fiber mass, toroid adhesive mass, toroid gas barrier mass, toroid axial straps mass, radial straps mass, and gore mass. The tension cone input parameters for this study are summarized in Table 3. A 30% mass margin was added to the final masses to account for any miscellaneous mass and uncertainty not accounted for in this analysis.

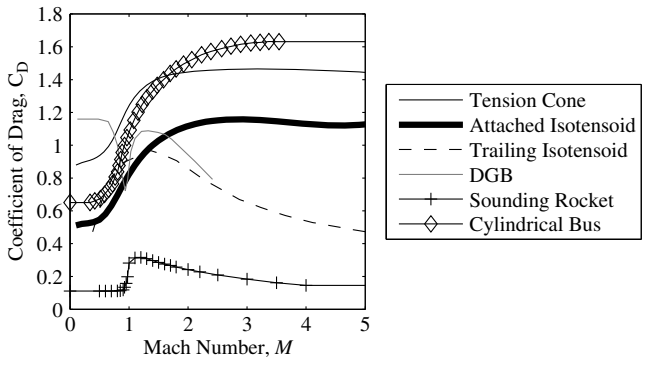

Fig. 3 Mach-dependent aerodynamics for the sounding rocket, vehicle bus, and decelerators.

Table 2 FUN3D parameters

Variable	Value	Units
M	4.0	— —
ρ	0.0577	kg/m^3
T_{ref}	219	K
V	1181	m/s

The trailing isotensoid mass was calculated using a relationship accounting for the structural and aerodynamic parameters that govern the decelerator efficiency [36]. This relation, shown in Eq. (1), accounts for the mass of meridian tapes, rise and suspension lines, and the canopy mass in the first and second terms, respectively:

$$m_{\text{Iso}} = bq_{\text{deploy}}(C_D A)^{3/2} + cd_f(C_D A) \tag{1}$$

The aerodynamic drag area $C_D A$ shown in Eq. (1) is of the trailing isotensoid only. The constants b and c, which were derived from pressure vessel theory, are specified by Anderson et al. to be 6.9×10^{-5} kg/N · m and 7.41, respectively [36]. Calculated from the baseline trajectory simulation, a dynamic pressure at deployment of 2 kPa was used. The final term d_f accounts for the areal density of the canopy fabric (kilograms per square meter). A 50% mass margin is added to final masses to account for miscellaneous mass and uncertainty not accounted for in this analysis.

The deployment mechanism for the trailing isotensoid requires a mortar similar to that of a typical parachute system [16]. The mortar mass required to eject a given trailing isotensoid was estimated from a linear regression of historical data for subsonic parachutes of similar masses, shown in Fig. 5.

IV. Decelerator Capability Assessment

To understand the impact SIAD deployment has on vehicle downrange distances, various payload masses (10–25 kg) and launch elevation angles (77–85 deg) were analyzed. Figure 6 shows downrange reduction performance, which is defined as the difference between the no-SIAD and SIAD deployment trajectories for a given launch and payload configuration. The larger the downrange reduction value, the more control authority the SIAD has for that configuration. Maximizing time in the atmosphere requires a reasonably high sounding rocket launch angle (81 deg), which reduces overall drag modulation capability due to the more vertical nature of the trajectory. For a given launch elevation angle, lower mass payloads (lower ballistic coefficient vehicles) exhibited a degradation in drag-modulated downrange performance. For a nominal atmosphere and drag coefficient profile, deployment of a tension cone SIAD at 45 km altitude provides a maximum 10.25 km reduction in downrange for the lowest launch elevation angle. Following the boost phase, the

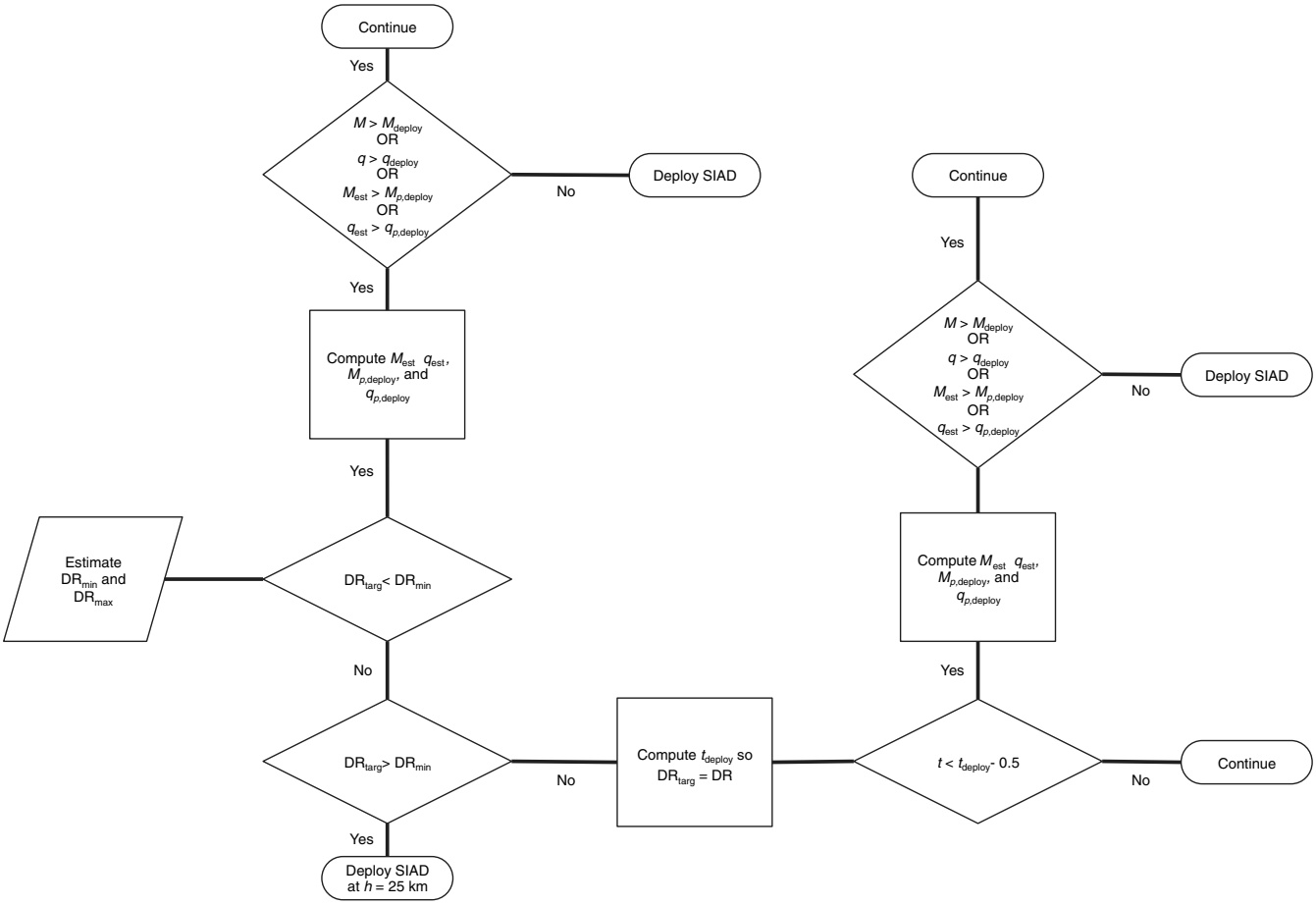

Fig. 4 Drag modulation predictor–corrector algorithm.

earlier the decelerator is deployed during the trajectory, the larger the drag modulation capability. As shown in Fig. 7, approximately 10 km of downrange modulation capability is achievable when deployed at 50 versus 25 km. It is assumed that the deployable can activate after apogee while still in the sample collection phase of flight.

The deployment conditions of the SIAD over a range of system configurations are shown in Fig. 7. The Mach number and dynamic pressures at deployment altitudes between 25 and 50 km for a variety of payload masses and launch elevation angles are shown to meet the deployment constraints of the IAD. Less severe deployment environments are experienced for lower mass systems.

Downrange capability was also examined as a function of decelerator drag area, as shown in Fig. 8. These trends were calculated using a launch elevation angle of 77 deg because this launch configuration provides the trajectory with the most horizontal flight path, which, in turn, maximizes the overall impact of drag modulation. As expected, the higher the SIAD is deployed, the more effective the downrange reduction performance (upward of 15 km for a 35 kg payload). However, as drag area is increased, a diminishing return on downrange modulation capability is experienced. As the deployment altitude is reduced, increasing the drag area of the decelerator is also shown to be less effective.

Table 3 Tension cone input parameters

Input parameter	Value
Dynamic pressure, Pa	2000
Number of toroid	1
Area ratio	6.39
Radius ratio	7
Diameter of torus circle, m	0.1125
Diameter of torus, m	0.7875
Vehicle bus diameter, m	0.356
Tension cone drag coefficient	1.5
Number of radial straps	16

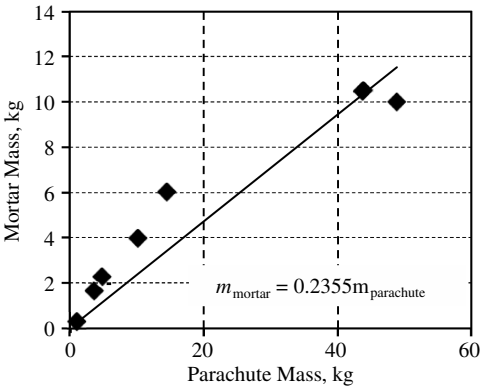

Fig. 5 Mortar mass regression [16].

The mass of each decelerator, attached to a 0.356-m-diam cylindrical bus, was estimated. Figure 9 shows the mass and storage volume estimates for all three SIAD configurations with coated Vectran material. Other SIAD material options exist. Heritage materials include Nomex and Nextel, whereas newer generation SIADs are typically made of Vectran and Kevlar or a coated variation of either material [16,37,38]. Adding a coating material to the fabric reduces fabric porosity and reduces friction within the fibers of the fabric [16]. As shown in Fig. 9b, the tension cone follows an exponential mass growth rate primarily due to the required onboard inflation system, which is dependent on torus volume. The mass trends for the trailing and attached isotensoid configuration follow nearly linear mass growth rates. It is important to note that the mass calculations for the tension cone include estimates of inflation

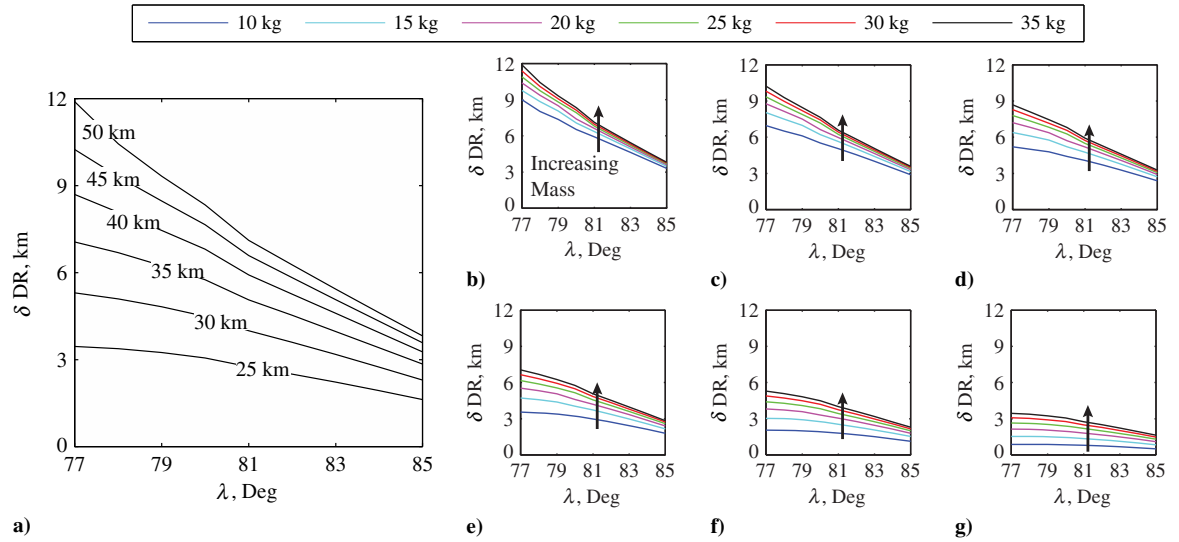

Fig. 6 Change in downrange using a 0.9 m diameter tension cone deployed at a) various altitudes for a 35 kg payload and for various payload masses deployed at b) 50, c) 45, d) 40, e) 35, f) 30, and g) 25 km.

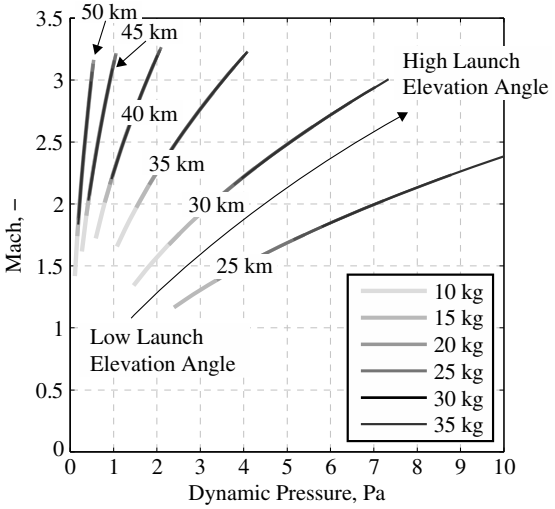

Fig. 7 Mach vs dynamic pressure at various deployment altitudes for a 0.9 m SIAD as a function of launch elevation angle and payload mass.

hardware, whereas the isotensoid calculations do not. Historical pre-inflation mechanisms have required on the order of a few fluid ounces of alcohol solution [17]. The trailing isotensoid mass must be summed with a deployment system mass expected to be on the order of 1 kg. Attachment and storage mechanisms are not included in the calculated mass estimates. Storage volume trends follow similar trends for each SIAD configuration, as shown in Fig. 9a. The trailing isotensoid requires more storage volume to account for the risers and towline.

The estimated mass values are comparable to historical test articles. The TD 5840 test article, consisting of a 1.5-m-diam attached isotensoid, had a fabric mass of 1.9 kg and was deployed at a dynamic pressure of 5.75 kPa [31]. The TD 6929 attached isotensoid test article, also 1.5 m in diameter, had a mass of 0.98 kg tested up to dynamic pressures of 28 kPa [39].

V. Uncertainty Analysis Results

A. Uncertainty Analysis

To investigate the overall performance improvement of the drag modulation implementation, Monte Carlo simulations were conducted for each decelerator configuration. Table 4 shows the

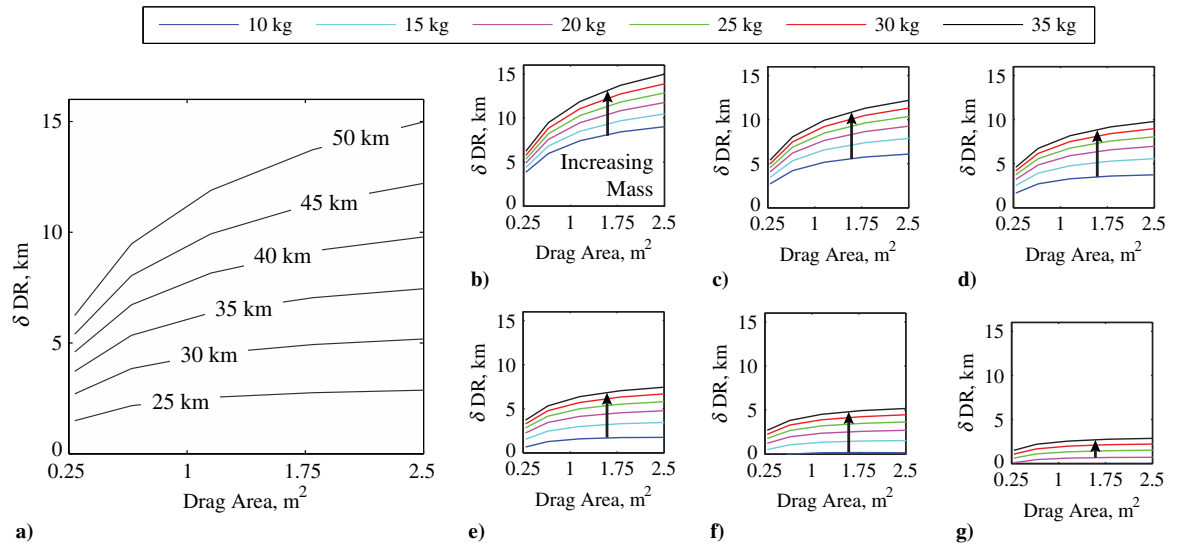

Fig. 8 Downrange reduction resulting from SIAD deployment at 77 deg elevation for a) various altitudes for a 35 kg payload and for various payload masses deployed at b) 50, c) 45, d) 40, e) 35, f) 30, and g) 25 km.

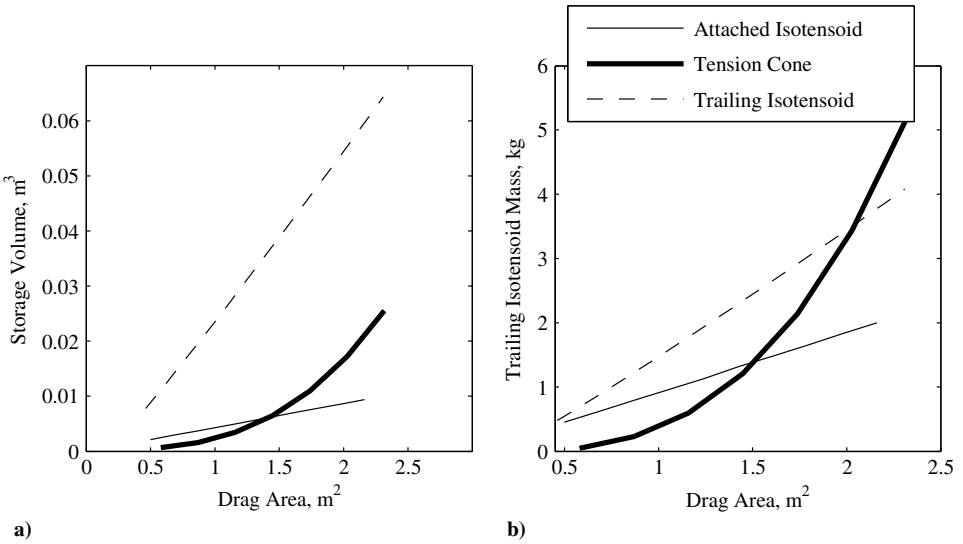

Fig. 9 Decelerator a) storage volume and b) SIAD mass as a function of decelerator drag area for coated Vectran material.

parameters, which were varied along with their nominal value, distribution type, and deviation value [40]. Earth-GRAM 2007 was used to generate all atmospheric information, including standard deviations as a function of altitude [34]. This study also estimated that the atmospheric dispersions generated from Earth-GRAM could be reduced to 10% of their original dispersions through use of weather balloons to provide detailed day-of-launch atmospheric data [41]. Figure 10 shows the reduced atmospheric density and eastward and northward wind variation as a function of altitude for the nominal White Sands launch site.

B. Monte Carlo Simulation Results

Three separate 1000-case Monte Carlo simulations were conducted for 1) an 8.5-m-diam DGB decelerator deployed at 73 km, 2) a 1.18 m^2 drag area SIAD deployed (corresponding to a 0.66-m-diam attached tension cone, 1.00-m-diam attached isotensoid, and 1.34-m-diam trailing decelerator) at 45 km, and 3) a 1.18 m^2 drag area SIAD deployed using the drag modulation algorithm (active between 25 and 45 km). Figure 11a shows the cumulative distribution functions (CDF) of range error for each system configuration. At the 95% confidence level, the DGB, IAD, and SIAD with drag modulation produce range errors, calculated as the root sum square of the downrange and cross-range values of 12.2, 11.6, and 9.7 km, respectively. This results in a 21% reduction in range error when a SIAD with drag modulation is implemented versus the stock option DGB decelerator. Implementation of drag modulation over a standard altitude deployment trigger of 45 km results in a 16% reduction in range error. If the dispersed range requirement of the parafoil is reduced to 5 km instead of 10 km, drag modulation has a much more significant impact on the dispersion results. Approximately 76% of the dispersed trajectories would land inside the reduced capability region, whereas the DGB and SIAD options would only achieve 55 and 61% success rates, respectively. Graphically, the impact of the drag-modulated SIAD on the downrange precision capability of the system is shown in Fig. 11b using probability density functions (PDF). Table 5 summarizes the statistics of the Monte Carlo analysis.

As shown in Fig. 12, at the 95% confidence level, the DGB's downrange/cross-range footprint at 6 km altitude is 30.2×9.2 km. The SIAD downrange/cross-range footprint is 29.1×1.2 km and, with the addition of drag modulation, the SIAD achieves a 22.2×2.0 km footprint. Although drag modulation reduced the downrange dispersion, a slight increase in cross-range dispersion is experienced as a result of the disparate altitudes of SIAD deployment. If deployed early in the trajectory, the vehicle is more susceptible to lateral motion due to winds because of longer flight times. Two parafoil capability regions, a 10 and a 5 km radius, represent various levels of performance of the guided parafoil. The larger radius region corresponds to a maximum capability region.

Cases that land within the parafoil capability regions, as shown in Fig. 12, have the ability to greatly increase landing precision to within 100 m. Conversely, cases that do not enter the parafoil capability region at an altitude of 6 km will not land near the designated target, resulting in recovery operations complexity and sample recovery time concerns. Figure 13 shows a comparison for each decelerator system configuration. The DGB and SIAD decelerator systems have comparable precision performance. Adding drag modulation with an SIAD reduces the dispersion by almost a factor of two. All three systems have at least 50% of their Monte Carlo runs land within the 5 km capability region. Overall, the 10 km capability region appears to be large enough to capture between 90 and 95% of the Monte Carlo cases, regardless of the decelerator system implemented.

Table 4 Monte Carlo simulation uncertainty models and parameters

Parameter	Nominal value	Distribution type	Deviation (3-sigma or min/max)
Atmosphere	10% Earth-GRAM, default settings for 32.38°N, 106.5°W on 1 June 2015	— —	— —
Launch elevation angle, deg	81.0	Uniform	±0.1
Launch azimuth angle, deg	355.0	Uniform	±0.1
Payload mass, kg	24.0	Uniform	±0.5
Mass drop time, s	10.0	Uniform	±1.0
Thrust multiplier (booster)	1.0	Gaussian	0.03 [40]
Thrust multiplier (sustainer)	1.0	Gaussian	0.03 [40]
Drag coefficient multiplier (sounding rocket)	1.0	Gaussian	0.1 [40]
Drag coefficient multiplier (payload bus)	1.0	Gaussian	0.1 [40]
Drag coefficient multiplier (decelerator)	1.0	Gaussian	0.1 [40]

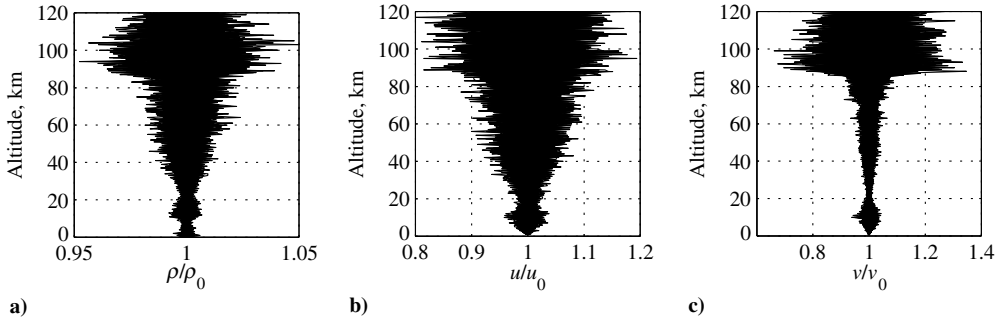

Fig. 10 Reduced uncertainties relative to Earth-GRAM of normalized a) density, b) eastward winds, and c) northward winds.

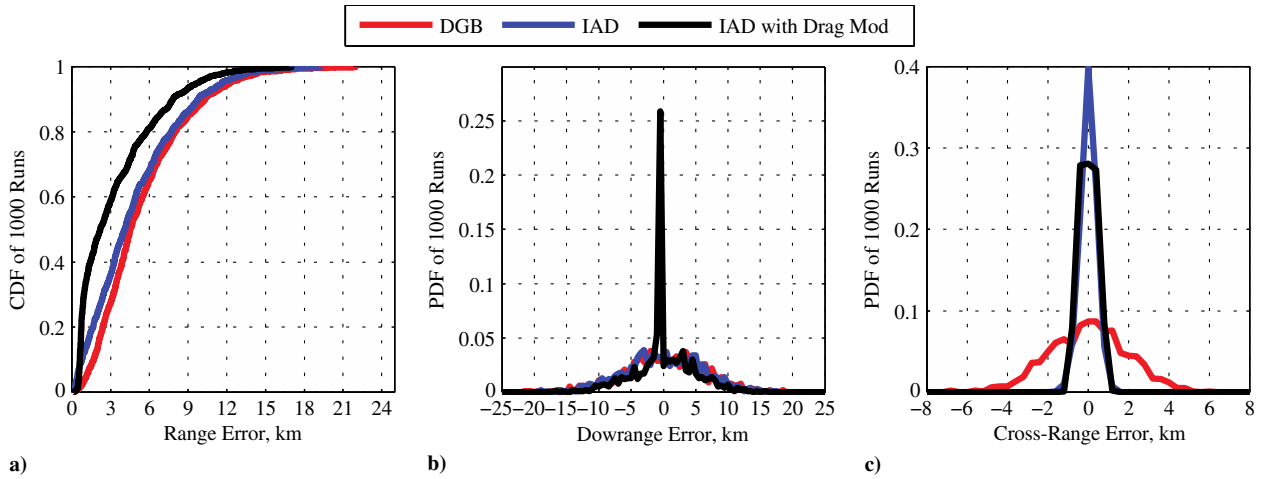

Fig. 11 Range error for all three architectures: a) CDF of the miss distance b) PDF of the downrange error, and c) PDF of the cross-range error.

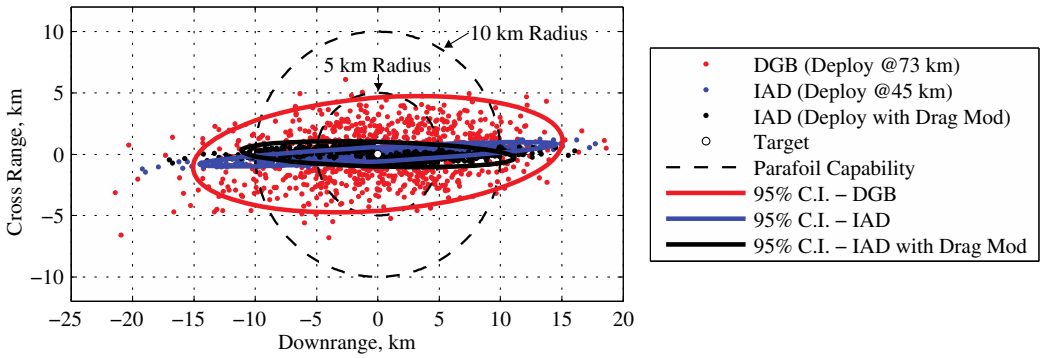

Fig. 12 Downrange/cross-range dispersions at 6 km altitude for DGB, IAD, and SIAD with drag modulation with associated 95% confidence interval dispersion ellipses.

VI. Conclusions

The objective of this study was to evaluate three SIAD configurations and the effect of SIAD-implemented drag modulation on a sounding rocket payload for atmospheric sample capture. A tension cone, attached isotensoid, and trailing isotensoid SIAD were investigated. Each SIAD configuration was evaluated considering mass, aerodynamic performance, and vehicle integration. In terms of aerodynamic performance, the tension cone SIAD is the preferred choice for the sizes investigated. The attached isotensoid was shown to be the most mass efficient decelerator, whereas the trailing isotensoid was found to be ideal from a vehicle integration perspective. Heritage test vehicles have repeatedly proven the trailing isotensoid

Table 5 Monte Carlo range error statistics

Architecture	50% confidence interval range error, km	75% confidence interval range error, km	99% confidence interval range error, km	Mean error, km	Standard deviation, km
DGB	4.53	7.31	16.70	5.40	3.52
IAD	4.10	6.78	15.21	4.79	3.53
IAD with drag modulation	2.20	4.88	13.31	3.33	3.11

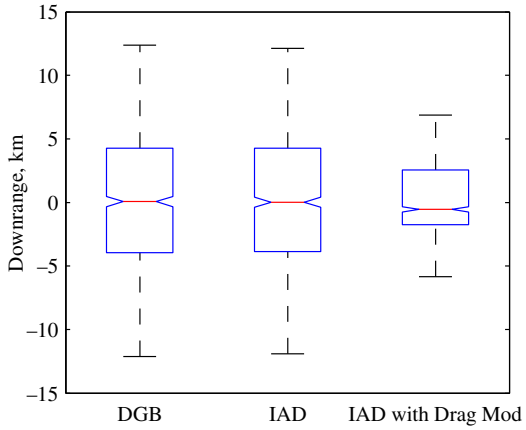

Fig. 13 Downrange dispersions for each decelerator system.

integration and deployment system. Across all metrics considered, the trailing isotensoid was deemed preferable for this mission.

Use of a SIAD for downrange control was then demonstrated and deployment conditions were characterized across a wide variety of vehicle and environmental parameters. For the reference trajectory, range error using drag modulation is reduced by 21% over existing DGB decelerators. Drag modulation control authority was shown to improve as payload mass increased and sounding rocket launch elevation angle decreased. Ninety-five percent of the SIAD drag modulation cases were shown to terminate within the 10 km parafoil capability region. Coupled with a guided parafoil, these cases reach the ground within 100 m of the target. Use of a SIAD, with or without drag modulation, was also found to ensure satisfactory deployment conditions of a guided parafoil.

Acknowledgments

The work presented was funded by the Charles Stark Draper Laboratory, Inc. under a University Research and Development project entitled "Deployable Decelerators for Small Atmospheric Recovery Missions." The authors would like to acknowledge Phil Hattis, Amer Fejzic, and Scott Thompson for their contributions to this investigation. The authors would also like to thank Christopher Cordell in the Space Systems Design Laboratory at Georgia Institute of Technology for contributions to the aerodynamics analysis presented in this work.

References

[1] Smith, B. P., Tanner, C. L., Mahzari, M., Clark, I. G., Braun, R. D., and Cheatwood, F. M., "Historical Review of Inflatable Aerodynamic Decelerator Technology Development," *2010 IEEE Aerospace Conference Proceedings*, IEEE Publ., Piscataway, NJ, March 2010, pp. 1–18.

[2] Bloetscher, F., "Aerodynamic Deployable Decelerator Performance Evaluation Program—Phase II," Goodyear Aerospace Corp., U.S. Air Force Flight Dynamics Lab. TR-67-25, June 1967.

[3] "PEPP Ballute Design and Development," NASA CR-66585, Sept. 1967.

[4] Clark, I., Adler, M., and Rivellini, T. P., "Development and Testing of a New Family of Supersonic Decelerators," *AIAA Aerodynamic Decelerator Systems Conference*, AIAA, Reston, VA, 2013. doi:10.2514/6.2013-1252

[5] Levy, L. L., "Use of Drag Modulation to Limit the Rate at Which Deceleration Increases During Nonlifting Entry," Ames Research Center, NASA TN-D-319, Sept. 1961.

[6] Kuo, Z.-S., Liu, K.-C., and Chang, Y.-S., "Explicit Guidance of Ballistic Entry Using Improved Matched Asymptotic Expansions," *Transactions of the Japan Society for Aeronautical and Space Sciences*, Vol. 50, No. 168, 2007, pp. 121–127. doi:10.2322/tjsass.50.121

[7] Rose, P. H., and Hayes, J. E., "Drag Modulation and Celestial Mechanics," *Advances in the Astronautical Sciences*, Vol. 8, Plenum Press, New York, 1963, pp. 178–187.

[8] Putnam, Z. R., and Braun, R. D., "Precision Landing at Mars Using Discrete-Event Drag Modulation," *Journal of Spacecraft and Rockets*, Vol. 51, No. 1, Jan. 2014, pp. 128–138. doi:10.2514/1.A32633

[9] Turco, R. P., Toon, O. B., Whitten, R. C., Keesee, R. G., and Hollenbach, D., "Noctilucent Clouds: Simulation Studies of Their Genesis, Properties and Global Influences," *Planetary and Space Science*, Vol. 30, No. 11, 1982, pp. 1147–1181. doi:10.1016/0032-0633(82)90126-X

[10] Goldberg, R. A., Pfaff, R. F., Holzworth, R. H., Schmidlin, F. J., Voss, H. D., Tuzzolino, A. J., Croskey, C. L., Mitchell, J. D., Friedrich, M., and Murtagh, D., "DROPPS: A Study of the Polar Summer Mesosphere with Rocket, Radar and Lidar," *Geophysical Research Letters*, Vol. 28, No. 8, 2001, pp. 1407–1410. doi:10.1029/2000GL012415

[11] Mathews, J. D., Janches, D., Meisel, D. D., and Zhou, Q. H., "Micrometeoroid Mass Flux into the Upper Atmosphere: Arecibo Results and a Comparison with Prior Estimates," *Geophysical Research Letters*, Vol. 28, No. 10, 2001, pp. 1929–1932. doi:10.1029/2000GL012621

[12] Soberman, R. K., "Extraterrestrial Dust Concentrations in the Upper Atmosphere," *Smithsonian Contributions to Astrophysics*, Vol. 11, 1967, pp. 323–331.

[13] Saunders, R. W., and Plane, J. M. C., "Laboratory Study of Meteor Smoke Analogues: Composition, Optical Properties and Growth Kinetics," *Journal of Atmospheric and Solar-Terrestrial Physics*, Vol. 68, No. 18, Dec. 2006, pp. 2182–2202. doi:10.1016/j.jastp.2006.09.006

[14] Miller, M. J., Steinfeldt, B. A., and Braun, R. D., "Mission Architecture Considerations for Recovery of High-Altitude Atmospheric Dust Samples," *AIAA Atmospheric Flight Mechanics (AFM) Conference*, AIAA, Reston, VA, 2013. doi:10.2514/6.2013-4604

[15] "NASA Sounding Rocket Program Handbook," Sounding Rockets Program Office; Suborbital and Special Orbital Projects Directorate, 810-HB-SRP, June 2005.

[16] Clark, I. G., Hutchings, A. L., Tanner, C. L., and Braun, R. D., "Supersonic Inflatable Aerodynamic Decelerators for Use on Future Robotic Missions to Mars," *Journal of Spacecraft and Rockets*, Vol. 46, No. 2, March 2009, pp. 340–352. doi:10.2514/1.38562

[17] Barton, R. R., "Development of Attached Inflatable Decelerators for Supersonic Application," Goodyear Aerospace Corp., NASA CR-66613, May 1968.

[18] Usry, J. W., "Performance of a Towed, 48-Inch-Diameter (121.92-cm) Ballute Decelerator Tested in Free Flight at Mach Numbers from 4.2 to 0.4," Langley Research Center, NASA TN-D-4943, Feb. 1969.

[19] Hattis, P., Campbell, D., Carter, D., McConley, M., and Tavan, S., "Providing Means for Precision Airdrop Delivery from High Altitude," *AIAA Guidance, Navigation, and Control Conference and Exhibit*, AIAA, Reston, VA, 2012. doi:10.2514/6.2006-6790

[20] Benney, R., Meloni, A., Henry, M., Lafond, K., Cook, G., Patel, S., and Goodell, L., "Joint Medical Distance Support and Evaluation (JMDSE) Joint Capability Technology Demonstration (JCTD) and Joint Precision Air Delivery Systems (JPADS)," *Proceedings of the Special Operations Forces Industry Conference*, Tampa, FL, 2009, pp. 2–4.

[21] Ewing, E. G., Bixby, H. W., and Knacke, T. W., *Recovery System Design Guide*, Air Force Flight Dynamics Lab. (AFFDL) TR-78-151, Wright–Patterson AFB, OH, 1978.

[22] Coatta, D., Jurewicz, D. A., Tutt, B. A., Clark, I. G., and Rivellini, T., "Development and Testing of an 8m Isotensoid Supersonic Inflatable Aerodynamic Decelerator (SIAD)," *AIAA Aerodynamic Decelerator Systems (ADS) Conference*, AIAA, Reston, VA, 2013. doi:10.2514/6.2013-1328

[23] Chang, K. Y., "Pyrotechnic Devices, Shock Levels and Their Applications," *Pyroshock Seminar at the 9th International Congress on Sound and Vibration*, Orlando, FL, 2002.

[24] Sengupta, A., Steltzner, A., Witkowski, A., Rowan, J., and Cruz, J., "An Overview of the Mars Science Laboratory Parachute Decelerator System," *Aerospace Conference*, IEEE, Piscataway, NJ, March 2007, pp. 1–8. doi:10.1109/AERO.2007.352827

[25] Brown, G. J., Epp, C., Graves, C., Lingard, J. S., and Darly, M., "Hypercone Inflatable Supersonic Decelerator," AIAA Paper 2003-2167, 2003.

[26] Bohon, H., "Summary of the Development Status of Attached Inflatable Decelerators," *Second Aerodynamic Deceleration Systems Conference*, AIAA, Reston, VA, 1968. doi:10.2514/6.1968-929

[27] McCoy, R. L., "'Mc Drag'—a Computer Program for Estimating the Drag Coefficients of Projectiles," Ballistic Research Lab., ARBRL TR-02293, Feb. 1981.
[28] Munson, B. R., Young, D. F., and Okiishi, T. H., *Fundamentals of Fluid Mechanics*, Wiley, New York, 2006, p. 586, Figure 9.23.
[29] Silbert, M., "Deployment of a Spin Parachute in the Altitude Region of 260,000 ft," *Journal of Spacecraft and Rockets*, Vol. 20, No. 1, Jan. 1983, pp. 11–14.
doi:10.2514/3.28350
[30] Silbert, M., Moltedo, A., and Gilbertson, G., "High Altitude Decelerator Systems," *10th Aerodynamic Decelerator Conference*, AIAA, Reston, VA, 1989.
doi:10.2514/6.1989-882
[31] Bohon, H. L., and Miserentino, R., "Deployment and Performance Characteristics of 5-Foot-Diamter (1.5 m) Attached Inflatable Decelerators from Mach Number 2.2 to 4.4," Langley Research Center, NASA TN-D-5840, Aug. 1970.
[32] Toohey Massac, D., "Development of a Small Parafoil Vehicle for Precision Delivery," Master's Thesis, Dept. of Aeronautics, and Astronautics, Massachusetts Inst. of Technology, 2005.
[33] Steinbrenner, J. P., and Abelanet, J., "Anisotropic Tetrahedral Meshing Based on Surface Deformation Techniques," *Proceedings of the AIAA 45th Aerospace Sciences Meeting*, AIAA Paper 2007-0554, 2007.
doi:10.2514/6.2007-554
[34] Justus, C. G., and Leslie, F. W., "NASA MSFC Earth Global Reference Atmospheric Model—2007 Version," NASA TM-215581, 2008, p. 2010.
[35] Samareh, J. A., "Estimating Mass of Inflatable Aerodynamic Decelerators Using Dimensionless Parameters," *Eighth International Planetary Probe Workshop*, Paper IPPW-8-6B, 2011.
[36] Anderson, M. S., Bohon, H. L., and Mikulas, M. M., "Structural Merit Function for Aerodynamic Decelerators," NASA TN-D-5535, Langley Research Center, Nov. 1969.
[37] Niccum, R. J., Munson, J. B., and Rueter, L. L., "Investigation of Kevlar Fabric-Based Materials for Use with Inflatable Structures," NASA CR-2724, April 1977.
[38] Stein, J., Sandy, C., Wilson, D., Sharpe, G., and Knoll, C., "Recent Developments in Inflatable Airbag Impact Attenuation Systems for Mars Exploration," *44th AIAA/ASME/ASCE/AHS/ASC Structures, Structural Dynamics, and Materials Conference*, AIAA, Reston, VA, 2012.
doi:10.2514/6.2003-1900
[39] Willis, C. M., and Mikulas, M. M., "Static Structural Tests of a 1.5-Meter-Diameter Fabric Attached Inflatable Decelerator," NASA TN-D-6929, Oct. 1972.
[40] Smayda, M. G., and Goyne, C. P., "Dispersion Reduction for a Sounding Rocket Scramjet Flight Experiment," *Journal of Spacecraft and Rockets*, Vol. 49, No. 3, May 2012, pp. 522–528.
doi:10.2514/1.A32097
[41] Karlgaard, C. D., Beck, R. E., Derry, S. D., Brandon, J. M., Starr, B. R., Tartabini, P. V., and Olds, A. D., "Ares I-X Trajectory Reconstruction: Methodology and Results," *Journal of Spacecraft and Rockets*, Vol. 50, No. 3, May 2013, pp. 641–661.
doi:10.2514/1.A32345

R. Cummings
Associate Editor